



Since January 2020 Elsevier has created a COVID-19 resource centre with free information in English and Mandarin on the novel coronavirus COVID-19. The COVID-19 resource centre is hosted on Elsevier Connect, the company's public news and information website.

Elsevier hereby grants permission to make all its COVID-19-related research that is available on the COVID-19 resource centre - including this research content - immediately available in PubMed Central and other publicly funded repositories, such as the WHO COVID database with rights for unrestricted research re-use and analyses in any form or by any means with acknowledgement of the original source. These permissions are granted for free by Elsevier for as long as the COVID-19 resource centre remains active.



# Split T7 promoter-based isothermal transcription amplification for one-step fluorescence detection of SARS-CoV-2 and emerging variants

Taehwi Yoon<sup>a,1</sup>, Jiye Shin<sup>a,1</sup>, Hyun-Jung Choi<sup>b,\*\*</sup>, Ki Soo Park<sup>a,\*</sup>

<sup>a</sup> Department of Biological Engineering, College of Engineering, Konkuk University, Seoul, Republic of Korea

<sup>b</sup> Department of Laboratory Medicine, Chonnam National University Medical School and Chonnam National University Hospital, Gwangju, Republic of Korea

## ARTICLE INFO

### Keywords:

SARS-CoV-2  
Isothermal amplification  
Split T7 promoter  
Three-way junction  
Transcription  
Light-up RNA aptamer

## ABSTRACT

The negative global impact of the coronavirus disease pandemic has highlighted the crucial need for a rapid and convenient method of viral RNA detection. In this study, we report a novel method, termed as the split T7 promoter-based isothermal transcription amplification with light-up RNA aptamer (STAR), for one-pot detection of viral RNA. STAR uses a split T7 promoter that is applied to a three-way junction to mediate the selective transcription by the T7 RNA polymerase in the presence of target RNA. In addition, a light-up RNA aptamer is used for signal amplification. STAR can detect viral RNA in less than 30 min with high specificity and sensitivity. By testing of 60 nasopharyngeal SARS-CoV-2 samples, the STAR assay demonstrates an excellent sensitivity and specificity of 96.7% and 100%, respectively. Moreover, we provide experimental evidence of the broad applicability of this assay through the multiplex detection of SARS-CoV-2 variants (D614G mutation) and direct detection of bacterial 16S rRNA.

## 1. Introduction

In December 2019, a novel infectious respiratory RNA virus, severe acute respiratory syndrome coronavirus 2 (SARS-CoV-2), emerged and rapidly spread around the world (Zhu et al., 2020). As of March 2022, over 487 million people have been infected and 6.1 million have died. Additionally, variants of SARS-CoV-2 with the 23,403 A > G mutation (p. D614G), conferring greater infectivity and more rapid spread, have become predominant in various regions (Korber et al., 2020; Plante et al., 2021; L. Zhang et al., 2020; Ozono et al., 2021). Therefore, there is an urgent need for rapid detection of SARS-CoV-2 to isolate infected people in a timely manner and prevent further viral transmission (Kilic et al., 2020; Wang et al., 2020; Y. Zhang et al., 2020; Cai et al., 2021).

Currently, quantitative reverse transcription polymerase chain reaction (qRT-PCR) using various primer-probe sets for viral genes, such as RNA-dependent RNA polymerase (RdRp), envelope (E), and nucleocapsid (N) genes, is the gold standard for detecting SARS-CoV-2 (Carter et al., 2020; Corman et al., 2020). The limit of detection (LOD) of each primer set is  $10^0$ – $10^2$  viral copies/ $\mu$ L, and the LOD for 100% sensitivity is  $10^2$  viral copies/ $\mu$ L (Vogels et al., 2020). However, qRT-PCR requires a

thermocycler and takes a long time (1–2 d) because it is generally conducted in centralized laboratories (Petralia and Conoci, 2017). The reverse transcription step, which is indispensable, further complicates the procedure (Taylor et al., 2010).

Isothermal amplification methods such as strand displacement amplification, nucleic acid sequence-based amplification, loop-mediated isothermal amplification and exponential amplification reaction have been developed to overcome the limitations of temperature control-based methods and facilitate point-of-care testing (Li and Macdonald, 2015; Woo et al., 2020; Yuce et al., 2021; Carter et al., 2021). However, most isothermal amplification methods entail critical drawbacks: (i) an initial, temperature-controlled denaturation/annealing step is required, (ii) the design of primers is complicated, and (iii) the target is limited to short RNA targets such as microRNAs with a 3'-OH group. Moreover, optimizing reactions for multiple enzymes is challenging, necessitating multiple steps for detection (Yan et al., 2014). For SARS-CoV-2, most isothermal amplification methods also involve the reverse transcription of RNA, thus risking contamination as the generated cDNA and amplified DNA do not decompose easily (Fallahi et al., 2018). Contamination can interfere with the reaction and result in false

\* Corresponding author.

\*\* Corresponding author.

E-mail addresses: [hyunjung.choi@chonnam.ac.kr](mailto:hyunjung.choi@chonnam.ac.kr) (H.-J. Choi), [akdong486@konkuk.ac.kr](mailto:akdong486@konkuk.ac.kr) (K.S. Park).

<sup>1</sup> These authors contributed equally to this work.

positives. Therefore, a rapid, one-step isothermal amplification method is still needed for SARS-CoV-2 detection.

We focused on target detection using a three-way junction structure, which is very specific and can easily distinguish changes in target sequences (Lee et al., 2020; Murakami et al., 2012). By means of this structure, sequences dependent on the targets (mimic sequences) can be amplified instead of directly amplifying target sequences. A representative example is the signal-mediated amplification of RNA technology (SMART) (Wharam et al., 2001), which is based on the three-way junction structure and applied in the detection of various nucleic acid biomarkers with high sensitivity. However, despite its advantages, SMART requires two enzymes, DNA polymerase and RNA polymerase, thus generating non-specific signals even in the absence of target RNA. Moreover, the RNA polymerase reaction must be performed after the DNA polymerase reaction, thereby prolonging the reaction time and rendering a one-step reaction impossible.

In the present study, we developed a new isothermal nucleic acid amplification technology that can quickly detect SARS-CoV-2 while addressing the limitations of SMART. Split T7 promoter-based isothermal transcription amplification with light-up RNA aptamer termed as STAR is a three-way junction-based technology that can detect target RNA with one enzyme in a single step. Through systematic investigation of the T7 promoter, we found that the transcription reaction effectively occurs with the split T7 promoter at a ratio of 4:16. This feature was combined with the three-way junction structure and light-up RNA aptamers to achieve detection of the SARS-CoV-2 N gene in

less than 30 min at 37 °C without the need for initial denaturation and cooling steps. The practical applicability of the proposed strategy was evaluated by determining its detection performance in 60 clinical samples. Moreover, STAR was utilized for multiplex detection of the D614G mutation and N gene of SARS-CoV-2 in a single tube as well as for the direct detection of bacterial 16S rRNA without additional nucleic acid purification, thereby confirming the wide applicability of this method for nucleic acid biomarker detection.

## 2. Experimental section

This section with details is presented in supporting information.

## 3. Results

### 3.1. Design and construction of STAR

We designed a reaction that does not require fluorophore labeling and can detect target RNA using a single enzyme in one tube (Fig. 1). The STAR reaction includes three components: STAR DNA probes, T7 RNA polymerase, and fluorogenic dye. STAR uses two types of DNA probes. The first consists of a signal template (ST) and split T7-16 (ST-16). ST comprises a complementary sequence (yellow) of the Mango aptamer (a light-up RNA aptamer), a T7 promoter sequence (blue), and a complementary sequence capable of binding to half of the target RNA region (black). ST-16 is a partial sequence of the T7 promoter (16 nt; blue) and

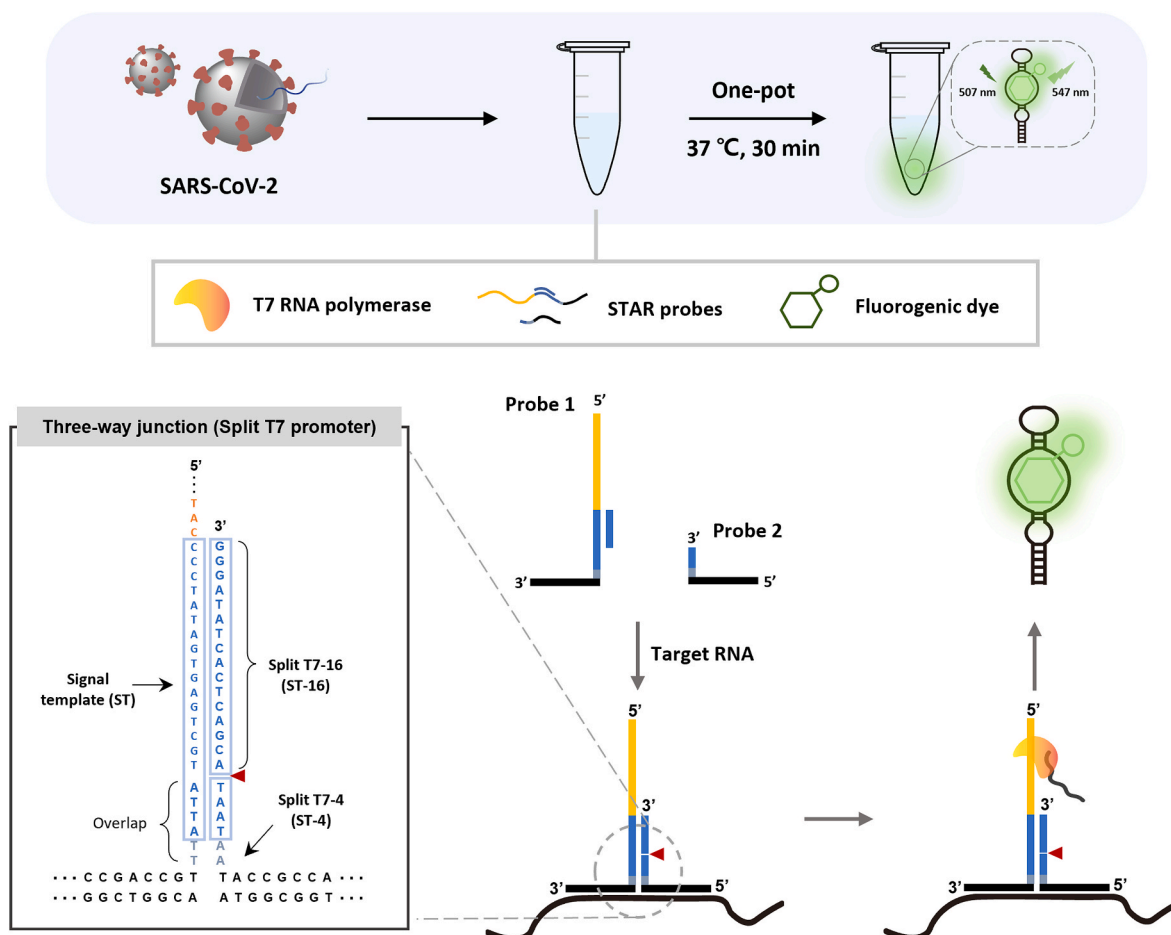


**Fig. 1. Schematic illustration of STAR for the detection of SARS-CoV-2.** In the presence of the target RNA, STAR DNA probes can form a three-way junction structure and complete the double-stranded T7 promoter with a nick site. Thus, T7 RNA polymerase can bind to the T7 promoter and initiate transcription for the generation of a large amount of light-up RNA aptamers. Subsequently, the light-up RNA aptamers combine with the fluorogenic dye, resulting in the generation of a highly enhanced fluorescent signal. The one-step reaction occurs at 37 °C within 30 min.

is hybridized to the T7 promoter sequence of the ST. The second probe is split T7-4 (ST-4), consisting of a partial sequence of the T7 promoter (4 nt; blue) and a sequence capable of binding to the other half of the target RNA region (black).

All STAR reactions are performed at 37 °C. The STAR DNA probes are designed not to hybridize when target RNA is absent because the 5'-ATTATT-3' sequence in the ST overlap has a  $T_m$  of only 12 °C. Therefore, the three-way junction structure that mediates double-stranded T7 promoter formation cannot be established. In contrast, the target RNA preferentially binds to the ST and ST-4 complementary sequence. Accordingly, the overlap part (5'-ATTATT-3') of ST is brought in proximity to ST-4 (5'-AATAAT-3') and can hybridize, resulting in three-way junction formation and completion of the double-stranded T7 promoter with a nick site. T7 RNA polymerase then binds to the double-stranded promoter and generates the Mango aptamer via transcription. Finally, the fluorogenic dye, TO1-biotin, binds to the Mango aptamer to generate an enhanced fluorescence signal. All processes take place in a single tube. All DNA probes were optimized using NUPACK (Zadeh et al., 2011) analysis to prevent unwanted binding between them (Table S1).

### 3.2. Optimization of split T7 promoter-based DNA probes and reaction conditions

Because the key step in STAR is the effective formation of the double-stranded T7 promoter with a nick site in the presence of target RNA via the induction of the three-way junction structure, we first investigated the best split ratio of the T7 promoter. The nick site was inserted sequentially from the 5' end of the T7 promoter to produce split promoters at various ratios (Fig. 2A). By placing the complementary sequence of the Mango aptamer within the template (T), transcription could be monitored by measuring the fluorescence signal of TO1-biotin. In the intact T7 promoter (0:20 split ratio), the addition of either T + SP2 or T + SP1 + SP2 resulted in effective transcription, as indicated by strong fluorescence. Moreover, when using a split T7 promoter at 1:19, the signal increased compared to that of the intact T7 promoter, despite the presence of the nick site (T + SP1 + SP2). Additionally, transcription occurred effectively in the presence of T + SP2. When the split ratio was changed from 2:18 to 4:16, transcription occurred effectively in the presence of T + SP1 + SP2, which harbors the nick site. However, in the case of T + SP2, which lacks sequences at the 5' end of the promoter, transcription was not effectively executed, as indicated by the decreased

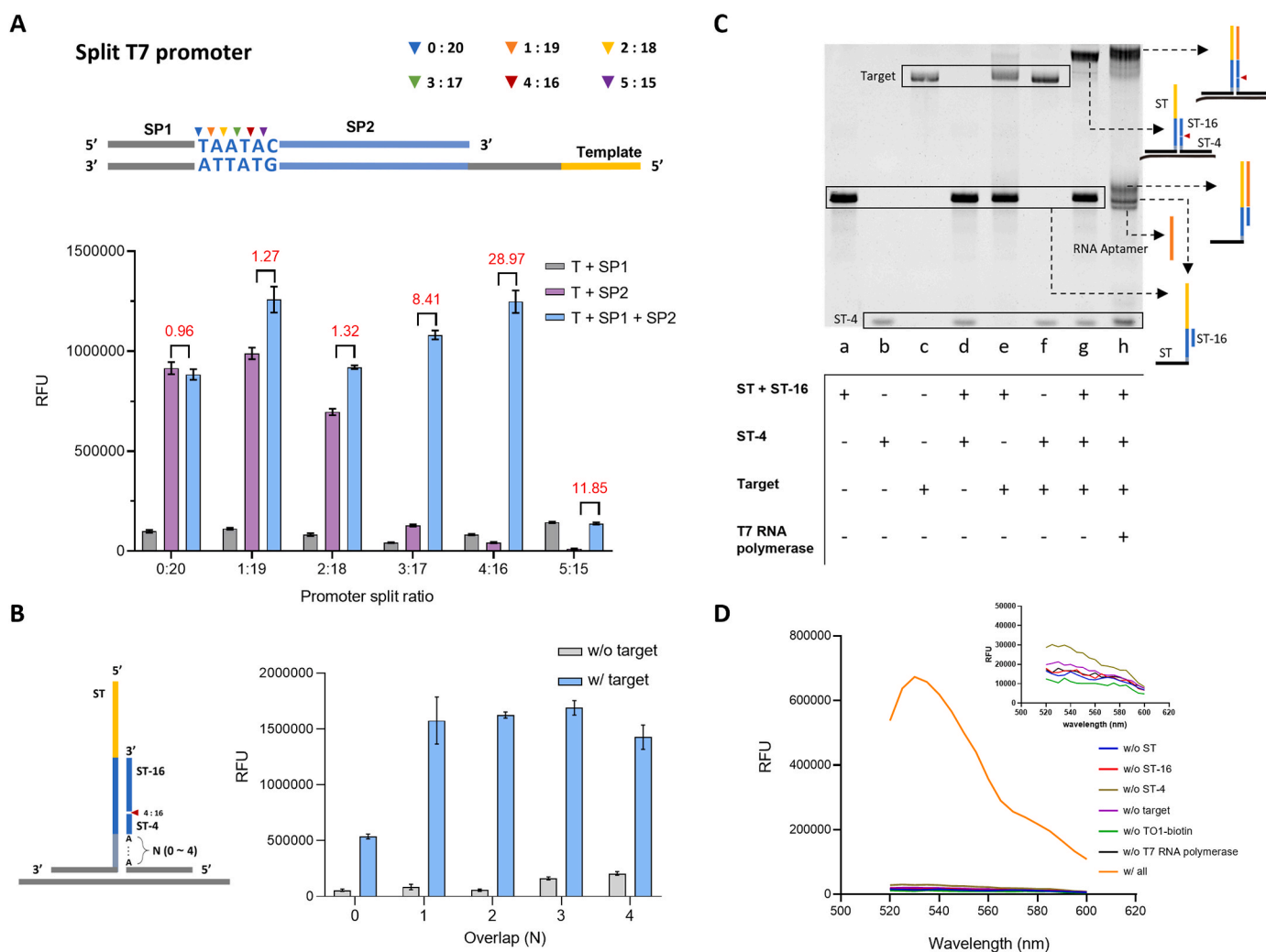


**Fig. 2. Construction and feasibility of STAR.** (A) Fluorescence signal of TO1-biotin after the transcription reaction with the split T7 promoter at different ratios (0:20, 1:19, 2:18, 3:17, 4:16, and 5:15). The combinations of template (T), split promoter 1 (SP1), and split promoter 2 (SP2) are shown. The fluorescence signal ratios of T + SP2: T + SP1 + SP2 are shown in red. (B) Optimization of overlap length. The split ratio of the T7 promoter was fixed at 4:16. The w/o and w/ indicate without and with, respectively. (C) Polyacrylamide gel electrophoresis results. The corresponding DNA probes are illustrated in each region. (D) Fluorescence emission spectra in various reaction conditions. The inset shows an expanded view of the fluorescence emission spectra of the reactions with various partial combinations of components.

fluorescence signal of TO1-biotin. Use of the 3:17 split ratio sharply decreased the fluorescence signal in the absence of SP1 (T + SP2), which implies that the three-nucleotide portion on the 5' side of the T7 promoter is important for specific recognition by T7 RNA polymerase, which then catalyzes transcription. Notably, the highest signal increase (28.97) in the presence of T + SP1 + SP2 relative to T + SP2 was observed using the 4:16 split ratio. In contrast, when the 5:15 split ratio was used, transcription rarely proceeded even if T, SP1, and SP2 were all present, indicating that T7 RNA polymerase does not recognize the T7 promoter when a nick site is located five nucleotides from the 5' end of the T7 promoter. Based on these results, the 4:16 split ratio was chosen for use in combination with the three-way junction structure.

Next, structural optimization for three-way junction formation was performed using the 4:16 split ratio. ST was designed to include a complementary sequence that binds half of the target RNA (black), the regions that hybridize to 16 nucleotides (ST-16) of the split T7 promoter (blue), and the complementary sequence for the Mango aptamer (yellow). Additionally, another split T7 promoter (ST-4) was designed to include four nucleotides of the T7 promoter (blue) and a complementary sequence that binds to the other half of target RNA (black). Only when the target RNA is present, the first probe, composed of ST and ST-16, and the second probe (ST-4) can combine to form the complete T7 promoter with a nick site. To achieve this, the Tm of ST and ST-4 was adjusted by including additional overlap sequences (0–4) (Fig. 2B). When the additional overlap sequence was not included (0 bp), a negligible fluorescence signal was produced in the absence of the target. In contrast, when the target was present, transcription was not effectively executed, which is attributed to the short overlap sequences (4 bp) between ST and ST-4. Notably, when one or more nucleotides of overlap sequences were added, strong fluorescence was obtained in the presence of the target. This confirmed that an overlap of at least 1 bp is required to stably form a three-way junction structure and induce transcription. However, when the additional overlap sequence exceeded 3 bp, non-specific transcription proceeded in the absence of a target. Therefore, the additional overlap was set at 2 bp with a total overlapping region of 6 bp (4 bp from T7 promoter).

### 3.3. Feasibility of STAR-mediated SARS-CoV-2 detection

Under the optimized conditions (Figs. S1–S5), we employed the N gene of SARS-CoV-2 as the target to confirm the detection efficacy of STAR (Tables S2 and S3). We first confirmed three-way junction structure formation in the presence of target RNA and the transcription reaction using polyacrylamide gel electrophoresis analysis. ST and ST-16 hybridized (a), whereas ST, ST-16, and ST-4 did not form the three-way junction structure in the absence of target RNA (d) (Fig. 2C). When all DNA probes and the target were present, the three-way junction structure was formed (g), and the presence of T7 RNA polymerase resulted in a large amount of light-up RNA aptamers being produced through transcription (h).

Next, the fluorescence spectra in the absence of each STAR component were evaluated (Fig. 2D). When either of the DNA probes (ST, ST-16, and ST-4) or the target was absent, the double-stranded T7 promoter and the Mango aptamer could not be generated. Thus, binding of the aptamer with TO1-biotin did not occur, and negligible fluorescence was observed. Additionally, there was no fluorescence in the absence of TO1-biotin or T7 RNA polymerase. Only when all elements were present, a high fluorescence signal was generated, indicating that all the elements of STAR play an indispensable role in the detection of target RNA. In addition, we evaluated the detection sensitivity by designing five sets of DNA probes against different regions (1–5) of the SARS-CoV-2 N gene (nucleotide positions 28,809–29,188). The results in Figs. S6–8 reveal that transcription efficiency was dependent on the targeted locus; accordingly, DNA probes against locus (L) 2 and 4 that exhibited greater fold changes were selected for use in subsequent experiments.

### 3.4. Targeting two loci to improve the detection sensitivity of STAR

To improve sensitivity, we used two probes simultaneously. As each STAR probe generates a signal by binding to the respective locus of target RNA, the overall signal can thus be further amplified. As shown in Fig. 3A, STAR probes targeting L2 and L4 were designed to be specific only to SARS-CoV-2. Agarose gel electrophoresis was first performed to verify that both STAR probes (L2 and L4) bind to the single target simultaneously. Electrophoretic mobility decreased when both probe sets were added (4) as compared to a single probe set (L2 or L4) (2 and 3), as confirmed by the higher band position (Fig. 3B), indicating that the two STAR probes specifically bound to their respective regions in the target RNA. Additionally, when both probe sets were used (L2 + L4), enhanced fluorescence was obtained (Fig. 3C), indicating the utility of this approach when target RNA concentration is low. The presence of target RNA was determined at levels as low as  $10^2$  copies/ $\mu$ L (167 aM) by targeting the two loci, resulting in approximately 600-fold greater sensitivity than that obtained by targeting a single locus, which was sufficient for SARS-CoV-2 detection in clinical settings (Fig. 3D). The specificity of STAR was then evaluated using DNA probes designed to not bind to six human coronaviruses, including other alphacoronaviruses and betacoronaviruses (Cimolai, 2020; Pyrc et al., 2007; Sizun et al., 2020). When RNAs from these coronaviruses (100 nM) were added, the fluorescence signals were similar to those observed in the non-target control (NTC), whereas highly enhanced fluorescence signals were generated even from 1 nM of the SARS-CoV-2 N gene (Fig. 3E), confirming high specificity.

### 3.5. SARS-CoV-2 detection in clinical samples

We next subjected 60 residual RNA samples extracted from nasopharyngeal and oropharyngeal specimens to detection via the STAR assay (Fig. 4A). Specimens were obtained from Chonnam National University Hospital (CNUH, Republic of Korea) and verified via qRT-PCR, as the gold standard for SARS-CoV-2 diagnosis (Table S4). The STAR assay was independently performed in a blinded manner, exhibiting a sensitivity of 96.7% and a specificity of 100% (Fig. 4B). Only one false-negative result was obtained, involving the sample having a high cycle threshold (Ct) value. Owing to the very low amount of RNA in this sample, it was not detected via our STAR method. The performance of the STAR assay was further evaluated by comparing the obtained fluorescence intensities to Ct values from qRT-PCR. As shown in Fig. 4C, the STAR assay results were consistent ( $R = 0.8393$ ) with those from qRT-PCR. Statistical analysis via the two-tailed Student's *t*-test (Fig. 4D) revealed that STAR can sufficiently distinguish positive from negative samples ( $P < 0.0001$ ). Finally, the area under the curve (AUC) from receiver operating characteristic (ROC) curve was determined to be 0.9878, which confirmed the excellent accuracy of the STAR method (Fig. 4E).

### 3.6. Multiplex STAR for detecting the SARS-CoV-2 D614G mutation and N gene

We selected the SARS-CoV-2 D614G mutation as an additional target to demonstrate the versatile applicability of STAR. Multiplex STAR for the simultaneous detection of D614G and the N gene in a single tube was subsequently performed. The D614G mutation is present in all SARS-CoV-2 variants, including alpha, beta, delta, and omicron (Cimolai, 2020). As an adenine (A) is substituted to a guanine (G) at position 23,403 of the SARS-CoV-2 genomic RNA, a specific STAR probe was designed to target this variant. For the multiplexing experiment, malachite green aptamer (Kolphashchikov, 2005) and fluorogenic dye (malachite green) were introduced, as these exhibit different excitation/emission wavelengths than those of the Mango aptamer/TO-1 biotin combination (Fig. 5A). First,  $\Delta G_{\text{wild type}} - \Delta G_{\text{mutant}}$  ( $\Delta\Delta G$ ) and the combination probability of the STAR probes for each

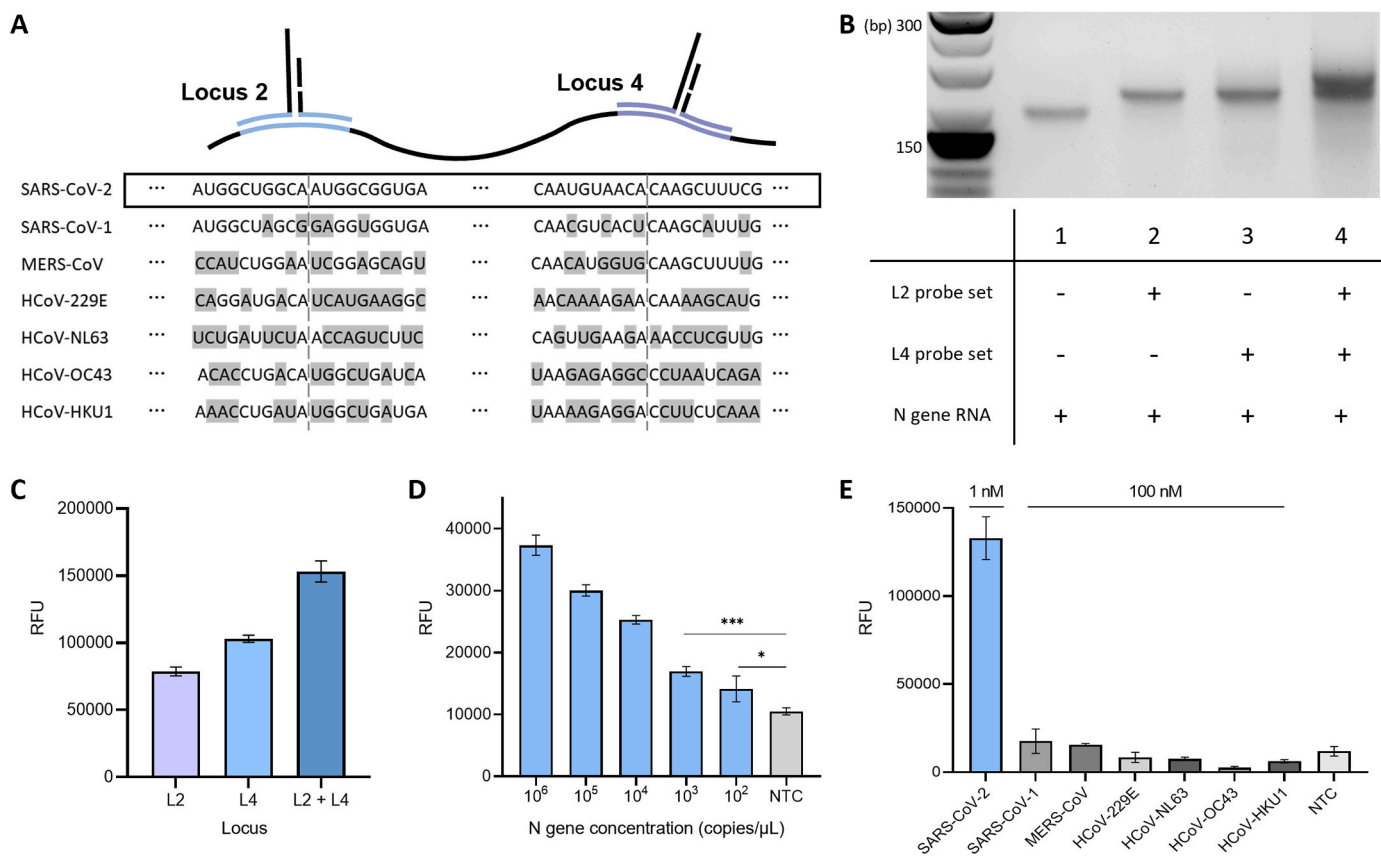


**Fig. 3. Combination of two STAR probe sets to improve detection sensitivity.** (A) Schematic of two different loci of the SARS-CoV-2 N gene and other human coronaviruses. The nucleotides in other viral RNA sequences that differ from those of SARS-CoV-2 are highlighted in grey. (B) Agarose gel electrophoresis image of the STAR probe set with N gene RNA. (C) Fluorescence signals measured in the presence of the L2 probe set, L4 probe set, and both probe sets. The concentration of the target N gene RNA was 1 nM. (D) Limit of detection using a combination of STAR probe sets for L2 and L4 (\* $P < 0.05$ , \*\*\* $P < 0.001$ ). (E) Detection specificity of the STAR assay using two STAR probe sets (L2 and L4). The concentration of the SARS-CoV-2 N gene RNA was 1 nM and that of the other probe sets was 100 nM.

mutant target according to the mutation site were estimated through NUPACK analysis. The  $\Delta\Delta G$  was the same from N3 to N10, i.e., 4.75, and the 8th mutation site (N8) exhibited the highest combination probability with the mutant (G) (Table S5). However, N8 had a relatively high combination probability (1.6%) of binding to the wild-type target (A), which could lead to an increased chance for false-positive results. Therefore, we introduced an artificial mismatch to prevent the STAR probe from binding to the wild-type and to lower the background noise (Table S6). By considering  $\Delta\Delta G$  and the combination probabilities for each target (wild-type and mutant targets), a mismatch was introduced at the 4th position (N4). Next, different nucleobases (adenine (A), thymine (T), guanine (G), and cytosine (C)) at N4 were evaluated to identify the nucleobase conferring the greatest discrimination of mutant (D614G) from the wild-type. The results in Fig. 5B indicate that G at N4 minimized the background noise in the presence of the wild-type target while generating a high fluorescence signal in the presence of the mutant target (D614G). With the optimized STAR probe for D614G mutation detection, the mutant target was detected at a concentration as low as 100 fM (Fig. 5C). Additionally, mixtures of mutant/wild-type targets at different molar ratios (0, 0.1, 1, 10, 50, and 100%) were analyzed using the proposed STAR. The molar ratio at which the mutant target could be distinguished from the wild-type target was 0.1%, which is comparable or superior to the performance of other methods (Kwon et al., 2019), confirming the excellent specificity of STAR (Fig. 5D).

We also established multiplex STAR, with the Mango aptamer and malachite green aptamer corresponding to the N gene and D614G mutation in the S gene, respectively (Fig. 5E). The binding of TO1-biotin and malachite green to Mango and malachite green aptamers, respectively, produced distinct fluorescence emission spectra (green and red

color) without any interferences (Fig. 5F). Additionally, STAR probes for the N gene produced greatly enhanced fluorescence (green color) through the generation of Mango aptamers only when the SARS-CoV-2 N gene was present. In turn, the STAR probes for D614G mutation generated an enhanced fluorescence signal (red color) by forming malachite green aptamers only when the mutation was present, thus demonstrating the feasibility of multiplex analysis (Fig. 5G). Furthermore, the sensitivities for both targets were evaluated, confirming that the N gene and D614G mutation could be simultaneously analyzed even at 100 fM (Fig. 5H). It should be noted that the degree of fluorescence signal change according to the target concentration differed between TO1-biotin and malachite green, which might be due to the difference in the intrinsic fluorescence characteristics of two fluorogenic dyes. Finally, STAR could be applied to detect bacterial 16S rRNA directly using thermal lysis (Fig. S9), which would allow the detection of several pathogens to be streamlined in real-world, clinical situations.

#### 4. Conclusions

We developed the STAR assay as a simple and rapid alternative to traditional viral detection methods. We determined that the split T7 promoter applied to the three-way junction structure mediates isothermal transcription with an efficiency comparable to that of the original, intact T7 promoter. This finding enables the use of a single T7 RNA polymerase and a reaction time of only 30 min at 37 °C. By using STAR, we sensitively detected the SARS-CoV-2 N gene; moreover, the practical application of STAR was clinically validated in 60 patient samples. To the best of our knowledge, this is the first report wherein a split T7 promoter is applied to a three-way junction structure, which

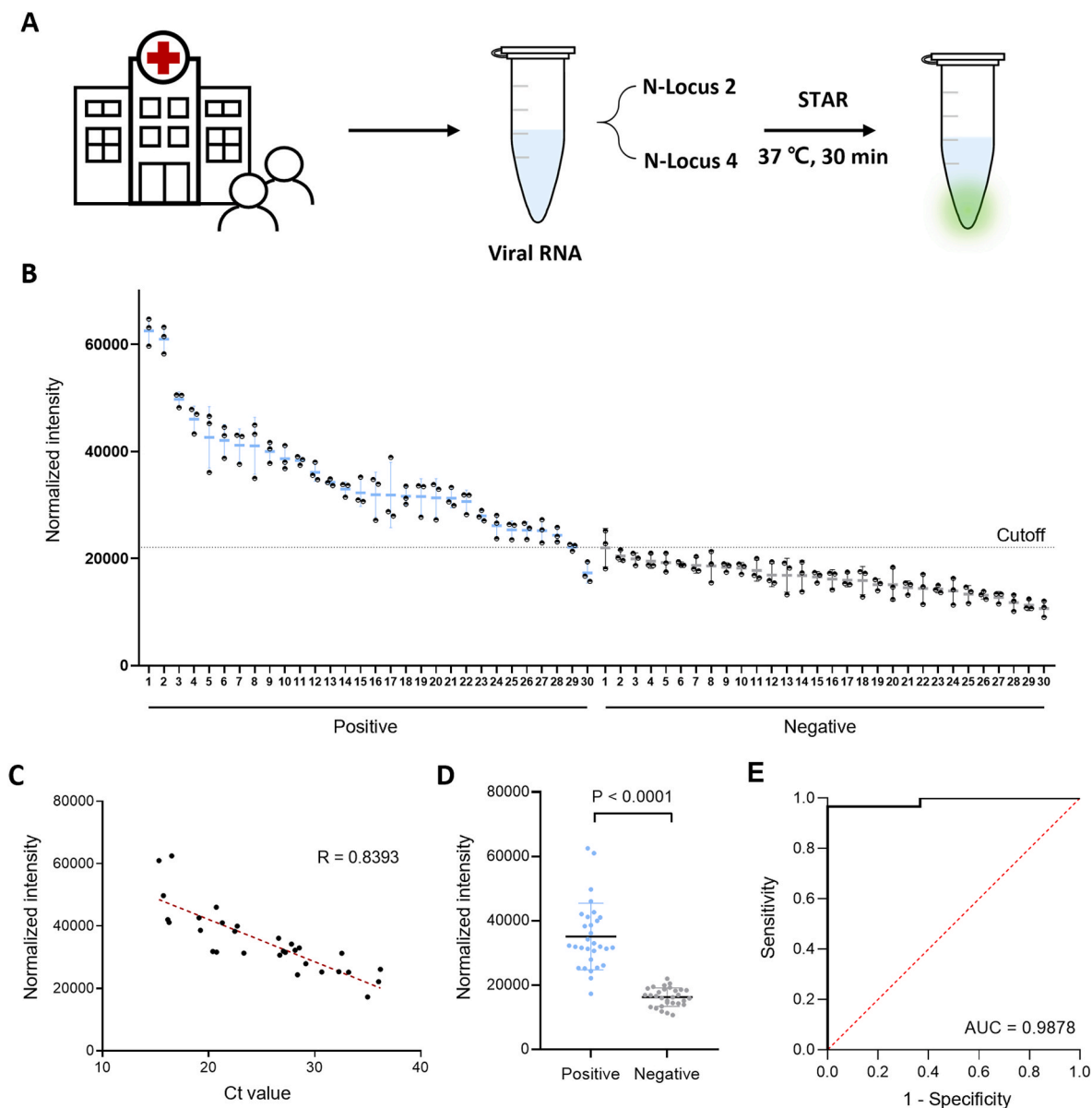


**Fig. 4.** Clinical validation of the STAR for SARS-CoV-2 diagnosis. **(A)** Schematic of SARS-CoV-2 detection via STAR. **(B)** SARS-CoV-2 detection in clinical samples. Thirty positive samples and thirty negative samples were tested. The cutoffs (dashed lines) were determined from the ROC curve. **(C)** Correlation of the STAR assay with clinical Ct values measured via qRT-PCR. **(D)** Statistically significant difference between positive and negative samples. **(E)** Receiver operating characteristic (ROC) curves of the STAR.

mediates selective transcription by T7 RNA polymerase only in the presence of target RNA. The significance of this work can be summarized as follows (full details including advantages over published methods (Table S7) can be found in the supplementary materials). (i) The proposed strategy requires only a single enzyme (T7 RNA polymerase), allowing for one-step, rapid detection (less than 30 min) of target RNA biomarkers. (ii) As light-up RNA aptamers are produced through transcription, the resulting fluorescence signal can be amplified without the need for expensive fluorophore labelling. (iii) By targeting two loci of SARS-CoV-2 simultaneously in a single reaction, the detection sensitivity was improved to  $10^2$  copies/ $\mu\text{L}$  (167 aM), which is sufficient for the detection of SARS-CoV-2 in a clinical setting. (iv) Excellent detection performance (sensitivity and specificity of 96.7% and 100%, respectively) was demonstrated through evaluation of 60 patient samples. Finally, (v) broad applicability was verified through the multiplex detection of the SARS-CoV-2 variants (D614G mutation) as well as through the direct detection of bacterial 16S rRNA without the need for

additional nucleic acid purification. Together, our findings highlight the potential of this novel technology for various applications in molecular biology and precision diagnostics.

#### Funding

This work was supported by the National Research Foundation of Korea (NRF) grant funded by the Korean government (Ministry of Science and ICT) [2020R1C1C1012275].

#### CRedit authorship contribution statement

**Taehwi Yoon:** Conceptualization, Methodology, Validation, Formal analysis, Writing – original draft. **Jiye Shin:** Conceptualization, Methodology, Validation, Formal analysis, Writing – original draft. **Hyun-Jung Choi:** Project administration, Writing – review & editing. **Ki Soo Park:** Conceptualization, Methodology, Funding acquisition, Project

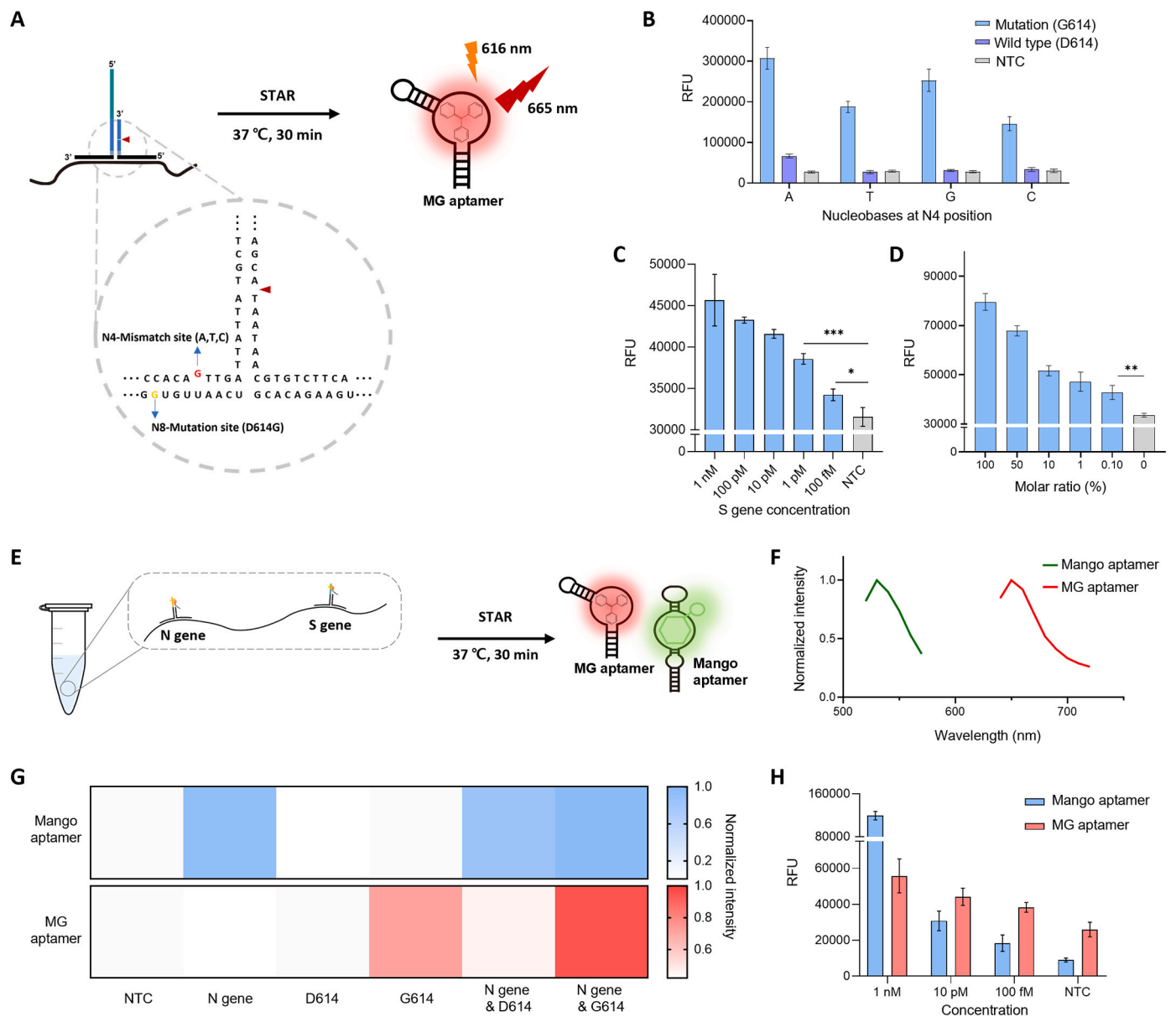


**Fig. 5. Application of STAR for the multiplex detection of the SARS-CoV-2 D614G mutation.** (A) Illustration of the STAR assay for the D614G mutation in the S gene of SARS-CoV-2. The mutation site is marked in yellow and the artificial mismatch is marked in red. (B) Malachite green (MG) signals obtained following STAR with DNA probes having different nucleobases (A, T, G, and C) at the N4 position. Tests were conducted in the presence of mutant (G) and wild-type (A) target or in the absence of a target (NTC). (C) Limit of detection of STAR for the D614G mutation (\* $P < 0.05$ , \*\*\* $P < 0.001$ ). (D) Detection of the D614G mutation in mixtures of mutant/wild-type targets with different molar ratios (\*\* $P < 0.01$ ). (E) Illustration of one-pot, multiplex STAR for simultaneous detection of the SARS-CoV-2 N gene and D614G mutation. (F) Normalized fluorescence emission spectra of TO1-biotin and MG, which bind to the Mango and MG aptamer, respectively. (G) Heatmap showing results of one-pot, multiplex detection of the N gene and D614G mutation. The fluorescence intensities were normalized against the maximum value. (H) One-pot, multiplex detection of the N gene and D614G mutation at different concentrations.

administration, Supervision, Writing – review & editing.

#### Declaration of competing interest

The authors declare that they have no known competing financial interests or personal relationships that could have appeared to influence the work reported in this paper.

#### Appendix A. Supplementary data

Supplementary data to this article can be found online at <https://doi.org/10.1016/j.bios.2022.114221>.

#### References

- Cai, Q., Mu, J., Lei, Y., Ge, J., Aryee, A.A., Zhang, X., Li, Z., 2021. *Anal. Bioanal. Chem.* 413 (18), 4645–4654.
- Carter, J.G., Orueta Iturbe, L., Duprey, J.H.A., Carter, I.R., Southern, C.D., Rana, M., Whalley, C.M., Bosworth, A., Beggs, A.D., Hicks, M.R., Tucker, J.H.R., Dafforn, T.R., 2021. *Proc. Natl. Acad. Sci. U.S.A.* 118 (35).
- Carter, L.J., Garner, L.V., Smoot, J.W., Li, Y., Zhou, Q., Saveson, C.J., Sasso, J.M., Gregg, A.C., Soares, D.J., Beskid, T.R., Jervey, S.R., 2020. *ACS Cent. Sci.* 6 (5), 591–605.
- Cimolai, N., 2020. *J. Med. Virol.* 92 (10), 1834–1844.
- Corman, V.M., Landt, O., Kaiser, M., Molenkamp, R., Meijer, A., Chu, D.K., Bleicker, T., Brünink, S., Schneider, J., Schmidt, M.L., Mulders, D.G., 2020. *Euro Surveill.* 25 (3), 2000045.
- Fallahi, S., Moosavi, S.F., Karimi, A., Chegeni, A.S., Saki, M., Namdari, P., Rashno, M.M., Varzi, A.M., Tarrahi, M.J., Almasian, M., 2018. *Diagn. Microbiol. Infect. Dis.* 91 (1), 6–12.

- Kilic, T., Weissleder, R., Lee, H., 2020. *iScience* 23 (8), 101406.
- Kolpashchikov, D.M., 2005. *J. Appl. Comput. Sci.* 127 (36), 12442–12443.
- Korber, B., Fischer, W.M., Gnanakaran, S., Yoon, H., Theiler, J., Abfalterer, W., Hengartner, N., Giorgi, E.E., Bhattacharya, T., Foley, B., Hastie, K.M., 2020. *Cell* 182 (4), 812–827.
- Kwon, W.Y., Cha, B.S., Kim, S., Hwang, S.H., Kim, J.M., Kalimuthu, K., Park, H.G., Park, K.S., 2019. *Analyst* 144 (14), 4149–4152.
- Lee, S., Jang, H., Kim, H.Y., Park, H.G., 2020. *Biosens. Bioelectron.* 147, 111762.
- Li, J., Macdonald, J., 2015. *Biosens. Bioelectron.* 64, 196–211.
- Murakami, T., Sumaoka, J., Komiyama, M., 2012. *Nucleic Acids Res.* 40 (3), e22 e22.
- Ozono, S., Zhang, Y., Ode, H., Sano, K., Tan, T.S., Imai, K., Miyoshi, K., Kishigami, S., Ueno, T., Iwatani, Y., Suzuki, T., Tokunaga, K., 2021. *Nat. Commun.* 12 (1), 848.
- Petralia, S., Conoci, S., 2017. *ACS Sens.* 2 (7), 876–891.
- Plante, J.A., Liu, Y., Liu, J., Xia, H., Johnson, B.A., Lokugamage, K.G., Zhang, X., Muruato, A.E., Zou, J., Fontes-Garfias, C.R., Mirchandani, D., 2021. *Nature* 592 (7852), 116–121.
- Pyrk, K., Berkhout, B., Van Der Hoek, L., 2007. *J. Virol.* 81 (7), 3051–3057.
- Sizun, J., Yu, M., Talbot, P., 2020. *J. Hosp. Infect.* 46 (1), 55–60.
- Taylor, S., Wakem, M., Dijkman, G., Alsarraj, M., Nguyen, M., 2010. *Methods* 50 (4), S1–S5.
- Vogels, C.B., Brito, A.F., Wyllie, A.L., Fauver, J.R., Ott, I.M., Kalinich, C.C., Petrone, M.E., Casanovas-Massana, A., Muenker, M.C., Moore, A.J., Klein, J., 2020. *Nat. Microbiol.* 5 (10), 1299–1305.
- Wang, C.J., Ng, C.Y., Brook, R.H., 2020. *JAMA* 323 (14), 1341–1342.
- Wharam, S.D., Marsh, P., Lloyd, J.S., Ray, T.D., Mock, G.A., Assenberg, R., McPhee, J.E., Brown, P., Weston, A., Cardy, D.L., 2001. *Nucleic Acids Res.* 29 (11), e54 e54.
- Woo, C.H., Jang, S., Shin, G., Jung, G.Y., Lee, J.W., 2020. *Nat. Biomed. Eng.* 4 (12), 1168–1179.
- Yan, L., Zhou, J., Zheng, Y., Gamson, A.S., Roembke, B.T., Nakayama, S., Sintim, H.O., 2014. *Mol. Biosyst.* 10 (5), 970–1003.
- Yuce, M., Filiztekin, E., Ozkaya, K.G., 2021. *Biosens. Bioelectron.* 172, 112752.
- Zadeh, J.N., Steenberg, C.D., Bois, J.S., Wolfe, B.R., Pierce, M.B., Khan, A.R., Dirks, R.M., Pierce, N.A., 2011. *J. Comput. Chem.* 32 (1), 170–173.
- Zhang, L., Jackson, C.B., Mou, H., Ojha, A., Peng, H., Quinlan, B.D., Rangarajan, E.S., Pan, A., Vanderheiden, A., Suthar, M.S., Li, W., 2020. *Nat. Commun.* 11 (1), 1–9.
- Zhang, Y., Xi, H., Juhas, M., 2020. *Trends Genet.* 37 (4), 299–302.
- Zhu, N., Zhang, D.Y., Wang, W.L., Li, X.G., Yang, B., Song, J.D., Zhao, X., Huang, B.Y., Shi, W.F., Lu, R.J., Niu, P.H., Zhan, F.X., Ma, X.J., Wang, D.Y., Xu, W.B., Wu, G.Z., Gao, G.F., Tan, W.J., 2020. *NEJM* 382, 727–733.